

TITLE: Recapitulation of endogenous 4R tau expression and formation of insoluble tau in directly reprogrammed human neurons

AUTHORS: Lucia S. Capano^{1,2,3,10}, Chihiro Sato^{4,10}, Elena Ficulle^{7,10}, Anan Yu^{8,10}, Kanta Horie⁴, Nicolas R. Barthelemy⁴, Susan G. Fox⁸, Celeste M. Karch^{5,6,9}, Randall J. Bateman^{4,5,6}, Henry Houlden⁷, Richard I. Morimoto⁸, David M. Holtzman^{4,5,6}, Karen E. Duff⁷, and Andrew S. Yoo^{1,2,6*}

¹Department of Developmental Biology, Washington University School of Medicine, St. Louis, Missouri, 63110, USA

²Center for Regenerative Medicine, Washington University School of Medicine, St. Louis, Missouri, 63110, USA

³Program in Molecular and Cell Biology, Washington University, St. Louis, Missouri, USA

⁴Department of Neurology, Washington University School of Medicine, St. Louis, Missouri, 63110, USA

⁵Knight Alzheimer's Disease Research Center, Washington University School of Medicine, St. Louis, Missouri, 63110, USA

⁶Hope Center for Neurological Disorders, Knight ADRC, St. Louis, Missouri, 63110, USA

⁷UK Dementia Research Institute at University College London, London, WC1E 6BT, UK

⁸Department of Molecular Biosciences, Rice Institute for Biomedical Research, Northwestern University, Evanston, Illinois, 60208, USA

⁹Department of Psychiatry, Washington University School of Medicine, St. Louis, Missouri, 63110, USA

¹⁰These authors contributed equally

*Correspondence: yooa@wustl.edu

SUMMARY

Tau is a microtubule-binding protein expressed in neurons and the equal ratio between 4-repeat (4R) and 3-repeat (3R) isoforms are maintained in normal adult brain function. Dysregulation of 3R:4R ratio causes tauopathy and human neurons that recapitulate tau isoforms in health and disease will provide a platform for elucidating pathogenic processes involving tau pathology. We carried out extensive characterizations of tau isoforms expressed in human neurons derived by microRNA-induced neuronal reprogramming of adult fibroblasts. Transcript and protein analyses showed miR-neurons expressed all six isoforms with the 3R:4R isoform ratio equivalent to that detected in human adult brains. Also, miR-neurons derived from familial tauopathy patients with a 3R:4R ratio altering mutation showed increased 4R tau and the formation of insoluble tau with seeding activity. Our results collectively demonstrate the utility of miRNA-induced neuronal reprogramming to recapitulate endogenous tau regulation comparable to the adult brain in health and disease.

INTRODUCTION

Tauopathies are adult-onset, neurodegenerative disorders whose shared pathology is intracellular tau protein aggregates (Gao et al., 2018; Götz et al., 2019). Tau, encoded by the Microtubule Associated Protein Tau (*MAPT*) gene, produces six protein isoforms whose expression is under strict developmental regulation, with only one isoform (0N3R) present during fetal development but all six present perinatally and maintained throughout lifespan (Goedert and Jakes, 1990; Goedert et al., 1989b; Hefti et al., 2018; Himmeler et al., 1989). Tau isoforms are defined by the inclusion or exclusion of three alternatively spliced exons: 2, 3, and 10. Exon 2 and 3 inclusion produces two N-terminal domains (N1 and N2) whereas exon 10 encodes the second imperfect-repeat microtubule-binding domain (R2) among three other

repeat domains (R1, R3, R4) (Goedert et al., 1989a). The inclusion or exclusion of exon 10 gives rise to 4-repeat (4R) and 3-repeat (3R) tau, respectively, and these two isoforms are expressed at an approximately 1:1 ratio in the healthy adult human brain (Goedert et al., 1989a; Kosik et al., 1989). Perturbation of the 3R:4R tau ratio contributes to the pathogenesis of various tauopathies, and out of the 53 known familial pathogenic tau mutations, almost 50% are located within or related to the expression of exon 10 (Ghetti et al., 2015). Thus, it is critical to establish a human neuron-based system that recapitulates the endogenous tau isoforms seen in the adult brain and tau pathology resulting from 3R:4R dysregulation in patient-derived neurons.

The past decade has primarily used neuronal differentiation of induced pluripotent stem cells (iPSCs) as the primary methodology for generating human neurons (iPSC-Ns). While these cells offer a robust means to generate neurons at a large quantity, their utility in studying processes that occur in aged neurons has been limited due to the reversion of the cellular age, and previous studies revealed iPSC-Ns represent fetal stages of development (Lapasset et al., 2011; Patterson et al., 2012) and express only marginal levels of 1N, 2N, and 4R tau expression (Ehrlich et al., 2015; Sato et al., 2018; Sposito et al., 2015). To increase 4R tau levels in iPSC-Ns, several experimental perturbations have been used including transgene overexpression (Verheyen et al., 2015), splicing mutations (Verheyen et al., 2018), or extended culturing times (188-365 days) (Beever et al., 2017; Sposito et al., 2015). However, these experimental manipulations still fall short of generating neurons with the endogenous ratio of 3R:4R in the adult human brain and highlight the need for an alternative strategy to generate human neurons that mirror the endogenous tau expression.

Brain-enriched microRNAs (miRNAs), miR-9/9* and miR-124 (miR-9/9*-124) are potent neuronal cell fate-defining miRNAs whose expression is present in fetal and adult brain, but in fetal brain they regulate cell proliferation and neuronal differentiation (Lim et al., 2005; Tan et al., 2012; Zhao et al., 2009). When these reprogramming effectors are ectopically expressed in human adult fibroblasts, they can directly convert fibroblasts to neurons (miNs) (Lu and Yoo, 2018; Yoo et al., 2011). The miRNA-induced neuronal state can be synergized with subtype-defining transcription factors (TFs) that guide conversion to specific neuronal subtypes (Abernathy et al., 2017; Victor et al., 2014). The fate transition occurs via miRNAs first instruct the erasure of fibroblast identity after the reprogramming cells enter the postmitotic state, followed by the neuronal program activation in sequence (Cates et al., 2020). The fate conversion relies on miRNAs targeting components of chromatin modifiers and transcription factors, coordinating extensive reconfiguration of chromatin landscape without passing through pluripotent and multipotent stem cell stages (Cates et al., 2020; Huh et al., 2016; Richner et al., 2015; Victor et al., 2018; Yoo et al., 2009). This property in turn allows for the maintenance of the epigenetic age signature of fibroblast donors (Huh et al., 2016). Additionally, modeling adult-onset disorders using miNs derived from symptomatic Huntington's disease patients exhibited hallmark adult-onset pathologies such as Huntingtin inclusion bodies, while their iPSC-N counterparts failed to do so (Victor et al., 2018).

Here, we reveal that miRNA-mediated direct reprogramming generates human neurons that express both 3R and 4R tau in the same ratio detected in adult human brains. RNA profiling by transcript assays and protein profiling by mass spectrometry demonstrates that adult human brain and miR-neurons from adult fibroblasts have indistinguishable 4R tau profiles, which starkly contrasts with the low 4R tau expression in primary fetal human neurons and iPSC-Ns. The endogenous tau isoform regulation in miR-neurons is sensitive to the point mutation within the splice site proximal to exon 10 in tauopathy patients resulting in reprogrammed neurons that showed increased 4R:3R tau ratio. Significantly, the increased level of 4R tau correlated with the formation of insoluble tau and seed-competent tau, reminiscent of that seen in human 4R tauopathies. We conclude that miRNA-mediated neuronal reprogramming provides a robust

model for studying both the normal and abnormal biology of tau and exon 10 pathological mutations.

RESULTS

MiNs display neuronal markers and express 4R tau

In this study, we adapted the neuronal conversion protocol based on miR-9/9*-124 and Neuronal Differentiation 2 (NEUROD2) and Myelin Transcription Factor 1 Like (MYT1L) transcription factors (TFs) to generate neurons of cortical lineage (Yoo *et al.*, 2011) (Fig 1). To minimize the number of lentiviruses used for transduction in fibroblasts, we replaced *NEUROD2* with ISX9, a neurogenic compound that has been previously shown to activate endogenous NEUROD-family TFs (Li *et al.*, 2015).

At thirty days post-induction (PID 30), immunostaining for a pan-neuronal marker Neuronal Cell Adhesion Molecule 1 (NCAM1) showed a robust reprogramming output with miNs displaying thin and branching processes (Fig. 1a left, middle-top: zoomed in view of NCAM1 expression). The reprogrammed cells were also enriched for another pan-neuronal marker, MAP2 (Microtubule Associated Protein 2) (Fig. 1a, middle-bottom). Beta III tubulin (TUBB3) was used to monitor cell morphologies (Fig. 1a, right). Importantly, immunostaining against tau revealed the miN population highly enriched with tau expression showing prototypical patterns of tau islands colocalizing with TUBB3-positive outer neurites (Fig. 1a, right and right-bottom zoomed image), an endogenous tau feature suggested to be reflective of tau-tau interactions (Siahaan *et al.*, 2019; Tan *et al.*, 2019).

Using immunocytochemistry on four independent fibroblast samples reprogrammed into miNs (Fig. 1b), approximately 60-70% of DAPI-positive cells showed MAP2- and tau-positivity, which is consistent with the reprogramming efficiency previously reported (Abernathy and Yoo, 2015; Cates *et al.*, 2020; Huh *et al.*, 2016; Victor *et al.*, 2014; Victor *et al.*, 2018). We also assayed expression of pan-neuronal genes by qPCR using primers for MAP2, *NEFL* (Neurofilament Light Chain), *MAPT*, and the glutamatergic marker, *SLC17A7* (also known as *VGLUT1*), showed enrichment in miNs over starting fibroblasts (Fig. 1c). Also, qPCR analyses of the cortical markers *TBR1* (T-Box Brain Transcription Factor 1), *MEF2C* (Myocyte Enhancer Factor 2C), *GRIN2C* (Glutamate Ionotropic Receptor NMDA Type Subunit 2c), *BRN2* (POU Class 3 Homeobox 2), and *NEUROD2* demonstrated that the combination of MYT1L and ISX9 are sufficient to drive cortical excitatory fate (Fig. 1d).

Using semi-quantitative PCR (sq-PCR) (Marone *et al.*, 2001) in which PCR is performed in a cDNA library with primers in exons 9 and 11, flanking exon 10, creating a long (4R) and short (3R) PCR product corresponding to the inclusion and exclusion of exon 10, respectively. We found consistent expression of 4R tau mRNA comparable to adult human brain samples (Fig. 1e), whereas all three types of fetal samples primarily expressed 3R tau (Fig. 1e, quantification in the right histogram). This confirms miNs do not lose the age of the starting cell during reprogramming, as then they would not express 4R tau isoforms as iPSC-Ns.

MiNs produce endogenous 4R tau protein similar to adult brain

To validate that mRNA expression led to protein expression, we performed mass spectrometry that can quantitatively and sensitively measure the tau isoforms in both cell culture and brain (Barthélemy *et al.*, 2020a; Barthélemy *et al.*, 2020b; Horie *et al.*, 2020; Sato *et al.*, 2018) on miNs from four independent adult individuals, four independent samples of fetal primary neurons or brain, adult brains from five individuals, and three iPSC-N replicates. We quantified tau peptides across full length intracellular tau protein, including peptides specific for

4R (residues 275-280, 282-290, and 299-317). In iPSC-Ns and fetal samples, the 1N, 2N and 4R peptides were expressed at less than 3% of the sum of all tau isoforms (i.e. 0N+1N+2N, and 3R+4R, respectively) (Fig. 2a-d), consistent with previous literature showing iPSC-Ns recapitulate only fetal neuronal tau isoforms (Ehrlich *et al.*, 2015; Sato *et al.*, 2018; Sposito *et al.*, 2015). Importantly, the 1N, 2N, and 4R peptide profiles of miNs showed significant enrichment over that of fetal samples, similar to the adult brain samples (Fig. 2a-d). To assay specific 3R:4R ratio in miNs, we analyzed the ratio of all three 4R-specific peptides to the adjacent, constitutive R1 domain peptide (260-267). Remarkably, miNs display an approximately 1:1 3R to 4R ratio equivalent to that of the adult human brain, which drastically contrasted iPSC-Ns and fetal neurons (Fig. 2a-b). The presence of multiple tau isoforms in miNs and adult brain was confirmed via western blot, which differed with fetal brain expressing only 0N3R isoform (Fig. 2d).

Using sqPCR we asked at what time point during the neuronal reprogramming tau expression begins, and in multiple fibroblast samples we found consistent, robust expression of both 3R and 4R tau transcripts at PID15 (Fig. 2e). Of note, this two-week point corresponds to the time that miNs start activating the neuronal program required for neuronal identity (Cates *et al.*, 2020). A timecourse of western blot for tau in miNs at days 15-24 into reprogramming showed clear expression of both 3R and 4R isoforms at 1:1 3R:4R ratio throughout the immunoblots (Fig. 2f).

Directly reprogrammed miNs from tauopathy patient fibroblasts recapitulate abnormal 4R tau expression

We next asked if the neuronal reprogramming would be sensitive to capture the increased 4R tau resulting from a point mutation at an intronic splice site known as IVS10+16 C>T (IVS10+16) (Hutton *et al.*, 1998), which disrupts a stem-loop structure and biases splicing towards exon 10 inclusion (Grover *et al.*, 1999). This familial mutation was shown to cause an approximately 2- to 4-fold increase in 4R tau mRNA (Connell *et al.*, 2005) and an imbalanced 3R:4R protein ratio, skewing towards increased 4R. We directly converted fibroblast samples with confirmed mutation status (Supp. Fig. 1, Supp. Table 1) from four symptomatic patients, first confirming their tau expression and successful neuronal conversion, with 75% of DAPI-positive cells expressing MAP2 and tau (Fig. 3a-b). Data from sq-PCR showed that IVS10+16 miNs had a significant increase in exon 10 inclusion over that of control miNs and adult brain (Fig. 3c, middle), with a 1.46-fold increase in their 4R:3R mRNA ratio (Fig. 3c, right).

Mass spectrometry analyses on IVS10+16 miNs and IVS10+16 iPSC-Ns demonstrated an increase in the 4R tau protein amount over the age-matched, control counterparts (Fig. 3d-e). The ratio of all three 4R-specific peptides showed a significant 1.31-1.41-fold increase in the IVS10+16 patient miNs over the control miNs (Fig. 3e-f). IVS10+16 iPSC-Ns also showed significant increase in 4R tau over control iPSC-Ns but far below that of the 3R tau level (Fig. 3d bottom, Fig. 3e). There was no significant difference in the profile of any other regions of tau including the ratio of 0N, 1N, or 2N isoforms between WT and IVS10+16 miNs (Fig. 3g).

Increased insoluble tau and seeding capacity in IVS10+16 miNs

Because an altered 3R:4R tau ratio is associated with aggregated tau in human tauopathies and adult-age is required for tau-associated phenotypes, we performed immunocytochemistry to assess whether insoluble tau accumulated in IVS10+16 miNs. Using methanol fixation method to remove soluble proteins (Guo *et al.*, 2016; Katsikoudi *et al.*, 2020) and a human-specific tau antibody, we observed thread-like tau staining (Braak and Del Tredici, 2010; Guo *et al.*, 2016; Katsikoudi *et al.*, 2020) in IVS10+16 miNs (Fig. 4a, top). When quantified, we observed a marked increase in tau staining over control miNs in all four of the

reprogrammed IVS10+16 miNs (Fig. 5a, bottom). This is in striking contrast to previously published data from IVS10+16 iPSC-Ns which were devoid of insoluble tau (Verheyen *et al.*, 2018). We further confirmed that the remaining tau signal was specific and caused by the tau protein by applying tau siRNA to IVS10+16 miNs. Total tau was reduced by 30-40% (Supp. Fig. 2), which led to significant reduction in the amount of insoluble tau (Fig. 5a).

Previous studies have indicated that pathological tau has seeding capacity that precedes the formation of insoluble tau (Holmes *et al.*, 2014) and which can be assayed using a tau-FRET Biosensor Assay (Clavaguera *et al.*, 2009; Frost *et al.*, 2009; Guo and Lee, 2011; Liu *et al.*, 2012). We found the patient-derived IVS10+16 miNs produced seeding-competent tau, with a 50% increase in FRET-positive signal from IVS10+16 miN lysate than that of control miN lysate and an over 300% increase in FRET intensity (Fig. 5b) indicating the presence of tau seeds.

DISCUSSION

The ability to study tau expression, isoform control, and age-associated disease pathologies will rely on a model system which endogenously recapitulates tau expression of the adult human brain. Results shown here provide thorough evidence at both transcript and protein levels that human neurons generated by miRNA-mediated neuronal reprogramming quickly and consistently mirror the adult ratio of 3R:4R matching that of the adult human brain. This ratio was strictly regulated in multiple independent donors. Using patient fibroblasts which harbor the IVS10+16 intronic mutation, we found that miRNA-reprogramming were sensitive to capture the difference in mRNA levels caused by the genetic mutation and the subsequent increase in 4R protein levels that reflect fold increase at mRNA level.

This human neuron model with robust 4R tau expression raises interesting future questions, for instance, which splicing factors drive exon 10 inclusion. Engineered mouse models expressing the entire human *MAPT* genomic sequence deviated from the expected 1:1 ratio of 3R:4R, and showed a bias towards 3R (Duff *et al.*, 2000), indicating there may exist splicing events and factors unique for 4R tau regulation in adult human neurons. Additionally, previous studies using tau minigenes to assay the regulation of tau exon 10 splicing in immortalized cell lines, has implicated over 100 putative splicing effectors including SRSF7 (Cavaloc *et al.*, 1994), SFPQ (Ishigaki *et al.*, 2017), NOVA1 (Wang *et al.*, 2004), and DYRK1A (Ding *et al.*, 2012), but these remain to be validated in an adult human neuronal context which could be addressed using miNs.

The maintenance of age is required for modeling adult-onset disorders supported by recently published recent study of age-associated phenotypes in patient-derived neurons (Mertens *et al.*, 2021; Victor *et al.*, 2018). IVS10+16 patient-derived miNs develop increased insoluble tau inclusions and seed-competent tau, two defining characteristics of pathological tau from adult-onset tauopathy brains (Frost *et al.*, 2009; Guo and Lee, 2011; Guo *et al.*, 2016). The ability for a model to endogenously produce pathogenic tau will provide a system for assaying the prevention and clearing of insoluble tau. Of note, the model responded to the genetic knock-down of tau using siRNA which has therapeutic implications as anti-sense oligomer directed reduction of tau is in human clinical trials (Safety, Tolerability and Pharmacokinetics of Multiple Ascending Doses of NIO752 in Progressive Supranuclear Palsy).

Given the global increase in the aging population and the correlating increase in tauopathies, a model system that mirrors the adult human brain and its tau expression will provide a novel avenue for studying these devastating diseases. The generation of human neurons that regulate tau splicing in the same way as the human adult brain and can replicate human tau-associated phenotypes represents a significant experimental advancement towards the investigation of tau-based pathology.

LIMITATIONS OF STUDY

While the data show that miNs provide an excellent model for studying tau isoform regulation and that they have the potential for testing pathological interventions in patient neurons, there is a limitation to direct reprogramming that should be noted. Scalability is limited due to tauopathy patient-derived fibroblasts being a rare commodity, especially those collected after symptom onset. This limitation highlights the need for more patient sample collection and availability to increase the scientific community's ability to leverage the benefit of direct neuronal conversion as an experimental system for adult-onset tauopathies.

ACKNOWLEDGEMENTS

The authors thank Edward D. Huey and Barbara Corneo (Columbia University) for providing one IVS10+16 fibroblast line, the Genome Technology Access Center and the fund from the Institute of Clinical and Translational Services (ICTS) (UL1TR002345) for their assistance in generating transcriptome dataset and iPSC lines, Mariana Beltcheva for iPSC to neuron differentiation, Kitra Cates and Dr. Seongwon Lee for qPCR primers, and Dr. Chloe He and Faris Shaikh for assisting with IP/MS experiments. This work was supported the following grants and awards. MCB training grant (T32 GM007067) (L.S.C.), ICTS JIT (JIT659H) (L.S.C and A.S.Y.), Farrell Family Fund for Alzheimer's Disease (A.S.Y, C.M.K., and D.M.H), NIH/NIA RF1AG056296, NIH/NINDS R01NS107488, Mallinckrodt Scholar Award (A.S.Y), NIH/NIA K01AG062796 (C.S.), SILQ Center (R.J.B.), NIH/NINDS R01 NS095773 (R.J.B.), NIH/NIA AG063521 (K.E.D and E.F) and the UK DRI funds from DRI Ltd, from the UK Medical Research Council, Alzheimer's Society and Alzheimer's Research UK (K.E.D and E.F), MRC and Wellcome Trust (H.H.), NIH R56 NS110890, Rainwater Charitable Organization (C.M.K.). ADRC Resources provided by Washington University Neuropathology core was supported by Healthy Aging and Senile Dementia [P01 AG03991], Alzheimer's Disease Research Center [P30 AG066444], Healthy Aging and Senile Dementia [P01 AG03991], Alzheimer Disease Research Center [P50 AG05691], and the Adult Children Study [P01 AG026276].

AUTHOR CONTRIBUTIONS

Conceptualization: A.S.Y., D.M.H., K.E.D., and L.S.C.; Methodology: A.S.Y. and L.S.C.; Investigation: L.S.C, C.S., E.F., A.Y., K.H., N.R.B., and S.G.F.; Validation: A.Y. and S.G.F.; Formal Analysis: L.S.C.; Writing – Original Draft: L.S.C. and A.S.Y.; Writing – Review & Editing: All authors.; Supervision: R.J.B., R.I.M, K.E.D, and A.S.Y.

DECLARATION OF INTERESTS

D.M.H. is as an inventor on a patent licensed by Washington University to C2N Diagnostics on the therapeutic use of anti-tau antibodies. D.M.H. co-founded and is on the scientific advisory board of C2N Diagnostics. C2N Diagnostics has licensed certain anti-tau antibodies to AbbVie for therapeutic development. D.M.H. is on the scientific advisory board of Denali, Genentech, and Cajal Neurosciences and consults for Genentech, Takeda, Casma, and Eli Lilly. K.H. is an Eisai-sponsored visiting researcher at Washington University and has received salary from Eisai. K.E.D is a board member and advisor for Ceracuity LLC. All other authors declare no competing interests.

FIGURE LEGENDS

Figure 1 | Directly reprogrammed neurons display exon 10 inclusion in mRNA.

(A) Representative images of miNs from healthy adult individuals (Ctrl 3+4) at post-induction day (PID) 30 immunostained with NCAM, MAP2, total tau, and TUBB3. Insets at the corners are immunostaining images performed in starting fibroblasts. Blue rectangular outlines depict the regions showed in magnified images. Scale bars = 50 μ m. **(B)** Left, representative images of control miNs stained for tau and TUBB3. Right, quantification of % positive over DAPI. Scale bars = 50 μ m. **(C)** Heatmap plots Z-scores comparing qPCR of neuronal genes between miNs and starting fibroblasts. **(D)** Fold change of cortical genes between starting fibroblasts and day 30 miNs. Mean \pm SEM.; two-tailed Student's t-test; *p < 0.05, **p < 0.01, ***p < 0.001. **(E)** Left, semi-quantitative PCR of 3R and 4R tau isoforms. Right: Quantification of 3R and 4R percent ratio of samples grouped by type and age. Mean \pm SEM; One-way ANOVA with multiple comparisons with post hoc Tukey's test; ***p < 0.001.

Figure 2 | MiN tau protein profile mirrors that of the adult human brain.

(A) Quantitation of relative tau peptides. Mean(thick line) \pm SEM. Pink and red dashed outline depicts 1N, 1N/2N, and 4R-specific tau peptides, respectively. **(B)** Quantification of 3R:4R isoform ratio. Mean \pm SEM; One-Way ANOVA with multiple comparisons and post hoc Tukey's test: Between any fetal vs adult sample for all three 4R peptides: ***p < 0.001. **(C)** Percent of N isoforms (calculation in methods). Mean \pm SEM; One-Way ANOVA with multiple comparisons and post hoc Tukey's test. All N isoforms between fetal vs control iPSC-Ns and between adult vs control miNs: ns p > 0.999; between control iPSC-Ns vs control miNs: 0N: **p = 0.002, 1N: **p = 0.002, 2N: *p = 0.015. **(D)** Western blot of tau isoforms. **(E)** Semi-quantitative PCR of 3R and 4R tau expression. Red rectangular outline depicts the time point when 4R tau starts being expressed consistently in multiple samples. Right, Two-tailed Student's T-test of PID15 vs PID20. Mean \pm SEM; ns p = 0.92. **(F)** Left, western blot of tau isoforms over reprogramming timecourse. Right, quantification of 3R:4R ratio of 0N and 1N isoforms during the time course of reprogramming. Mean \pm SEM; One-Way ANOVA with multiple comparisons and post hoc Tukey's test; Between fetal vs any miN: **p = 0.002; between fetal and adult: **p = 0.004.

Figure 3 | IVS10+16 patient-derived miNs show increased 4R tau mRNA and protein.

(A) Left, representative images of reprogrammed IVS10+16 miNs from four independent, symptomatic IVS10+16 patients, immunostained for tau and TUBB3. Right, Scale bars = 50 μ m. **(B)** Z score heatmap (from qPCR) representation of neuronal marker gene expression MAP2, NEFL, MAPT, and VGLUT1 in IVS10+16 miNs and starting fibroblasts. **(C)** Left, sqPCR for detecting 4R and 3R tau ratio. Middle: grouped intensity values for 3R and 4R from the sqPCR gel images. Mean \pm SEM. One-Way ANOVA with multiple comparisons and post hoc Tukey's test; Between control miNs vs IVS10+16 miNs and IVS10+16 miNs vs adult brain: ***p < 0.001. Right: fold changes in 4R expression normalized by control miN values. Mean \pm SEM; One-Way ANOVA with multiple comparisons and post hoc Tukey's test; Between control miNs vs IVS10+16 miNs: **p = 0.001; between IVS10+16 miNs vs adult brain: ***p < 0.001. **(D)** Quantitation of relative tau peptides. Mean(thick line) \pm SEM. **(E)** Quantification of 3R:4R isoform ratio. Mean \pm SEM. One-Way ANOVA with multiple comparisons and post hoc Tukey's test; control miNs vs IVS10+16 miNs: 275-280 **p = 0.004, 282-290 **p = 0.004, 299-317 **p = 0.008. Between any miN and iPSC-N: all peptides ***p < 0.001. **(F)** Fold change of 4R isoform expression for all three 4R-specific peptides over control miNs. **(G)** Percentage of N isoforms. Mean \pm SEM; One-Way ANOVA with multiple comparisons and post hoc Tukey's test. For all N isoforms: between control iPSC-Ns and IVS10+16 iPSC-Ns: ns p > 0.999; between control miNs

vs IVS10+16 miNs: 0N: ns p = 0.97; 1N: ns p = 0.983; 2N: ns p = 0.887; between IVS10+15 miNs vs IVS10+16 iPSC-Ns: 0N: *p = 0.038; 1N: *p = 0.027; 2N: ns p = 0.285.

Figure 4 | Formation of insoluble tau in IVS10+16 patient-derived miNs

(A-B) Representative images of IVS10+16 miNs and control miNs fixed in methanol, leaving only insoluble tau. Cells were co-labeled with MAP2 antibody (green) and total tau CP27 antibody (red). **(A)** Top, high magnification of IVS10+16 miNs and insoluble tau threads and tendrils. Bottom, arrowheads indicate the location of insoluble tau signals in control miNs (top) and IVS10+16 miNs (bottom). Left images: cells treated with control siRNA (siCtrl). Right images: cell treated with siRNA against total tau (siTotal tau). Right plot: Quantification of tau signals detected per DAPI signals in control miNs (WT miNs treated with siCtrl) in comparison to IVS10+16 miNs treated with siCtrl and IVS10+16 miNs treated with siTotal tau. n = 4 experimental replicates from three control and four IVS10+16 miNs. One-way ANOVA with multiple comparisons. ***p < 0.001. **(B)** Left, FRET signals for control and IVS10+16 miN lysate. Right, quantification of % FRET and Integrated FRET (from left). Student's t-test. *p < 0.05.

STAR METHODS

Supplemental Information Titles and Legends

Supplemental Figure 1 – Confirmation of mutational status in control and IVS10+16 fibroblasts

Supplemental Figure 2 – siRNA against total tau shows reduction in both mRNA and protein levels

Supplemental Table 1 – Fibroblasts, purchased samples, and oligonucleotide sequences used in experiments

Supplemental Table 2 – Antibodies used for experiments

Resource Availability

Lead Contact

Further information and requests for reagents may be directed to, and will be fulfilled by, the Lead Contact, Andrew S. Yoo (yooa@wustl.edu).

Materials Availability

All unique and stable reagents generated in this study are available from the Lead Contact with a completed Materials Transfer Agreement.

Methods and Materials

Fibroblast cell lines

Human fibroblasts were obtained from Coriell NINDS (AG04148, AG08260, AG08379, and AG13369), Columbia University (ES046), and University College London (UCL455, UCL457, and UCL497). The age, sex, and experiments each line were used for can be found in Supplemental Table 1. We do not have access to original patient data, and therefore cannot identify the donor. The research falls outside the federal definition under the jurisdiction of an institutional review board and is exempt from human subject studies.

Human brain samples

Three biological replicate lots of adult human brain RNA (R1234035-50) was purchased from BioChain. Fetal human brain RNA (#1F01-50) was purchased from Cell Applications Inc. Adult human brain samples include Novus purchased lysate (NB820-59177) and previously published control samples (age = 72-90, see Supplemental Table 1) obtained from Washington University

Alzheimer's Disease Research Center (ADRC) (Horie *et al.*, 2020). The study was approved by the Washington University Institutional Review Board, and all participants were consented for autopsy and sharing of samples. Fetal human neuron lysate (#1526) was purchased from ScienCell. Primary fetal neurons were purchased from ScienCell (#1520). Differentiated iPSC-derived Cortical Glutamatergic Neurons were purchased from BrainXell (#BX-0300).

Lentiviral Production

Lentiviruses were generated as previously described (Nuclear Reprogramming: Methods and Protocols, 2021) with minor changes. To make supernatant virus, viral supernatant was collected, spun at 1200g for 5min at 4°C, then passed through a 0.45uM filter. This supernatant was then aliquoted and directly frozen at -80°C until used (less than 1 year after production date).

Direct Neuronal Reprogramming

Human fibroblasts were directly reprogrammed to miNs as previously described(Nuclear Reprogramming: Methods and Protocols, 2021; Richner *et al.*, 2015; Yoo *et al.*, 2011) with slight modification. Briefly, fibroblasts were transduced with supernatant lentivirus mix comprised of dox-inducible miR-9/9*-124, rtTA, and the transcription factor MYT1L. From PID1 to PID14 cells were treated with DAPT (2uM) to increase neurite outgrowth and neuronal differentiation, and on PID 3, 6, 10, and 14, cells were also treated with the NEUROD1-activator ISX9 (10uM) to push cortical fate. Fibroblasts and reprogramming cells were cultured in DMEM+10%FBS through replating at PID5. On PID6, cells were switched to Neurobasal-A with B27+ (1000x) and Glutamax (500x), containing 1 µg/mL doxycycline, 200 µM dibutyl cyclic AMP, 1 mM valproic acid, 2uM DAPT, 200nM Ascorbic Acid, 10 ng/mL BDNF, 10 ng/mL NT-3, 1 µM retinoic acid, 10uM ISX9, 100x RVC, and 3 µg/mL puromycin. Cells were half fed every 4 days and doxed every 4 days on an offsetting 2 day scheduled. On PID14, miNs were half fed using BrainPhys containing N2A and SM1 (StemCell) with the following goodies: 1 µg/mL doxycycline, 200 µM dibutyl cyclic AMP, 1 mM valproic acid, 2uM DAPT, 200nM Ascorbic Acid, 10 ng/mL BDNF, 10 ng/mL NT-3, and 1 µM retinoic acid.

iPSC Generation and Genome Engineering

Dermal fibroblasts from MAPT IVS10+16 carriers (GIH36) were transduced with non-integrating Sendai virus carrying OCT3/4, SOX2, KLF4, and cMYC (Life Technologies) as previously described(Karch *et al.*, 2019). iPSC that were heterozygous for MAPT IVS10+16 were edited to WT (GIH36.2Δ1D01) using CRISPR/Cas9 as previously reported(Karch *et al.*, 2019). Mutation status was confirmed by Sanger sequencing. Cell lines were maintained in mTesR medium (StemCell Technologies) on Matrigel. Cell lines were confirmed to be free of mycoplasma.

iPSC Differentiation

MAPT IVS10+16 iPSC and isogenic controls were differentiated into neural progenitor cells (NPCs) as previously described(Jiang *et al.*, 2018; Karch *et al.*, 2019). Briefly, iPSC were dissociated with Accutase (Life Technologies). iPSC were then plated at 65,000 cells per well in Neural Induction Media (NIM; Stem Cell Technologies) in a 96-well v-bottom plate to form neural aggregates. After 5 days, neural aggregates were plated on Poly-L-Ornithine (PLO) and laminin-coated plates to form neural rosettes. After 5 to 7 days, neural rosettes were isolated by enzymatic selection and cultured as NPCs. NPCs were cultured on PLO and laminin-coated plates and terminal differentiation was initiated with the addition of cortical maturation medium (Neurobasal-A (Life Technologies) supplemented with B27 (Gibco), BDNF (Peprotech), GDNF (Peprotech), cAMP (Sigma) and L-glutamate (Sigma)). Neural cultures were maintained for six weeks.

Immunocytochemistry

Cells are fixed with either 4% PFA for 20min and washed 3x PBS after fixation. Fixed cells were permeabilized for 10min at RT in permeabilization buffer, blocked for 1hr RT in 5% BSA/1% NGS, then stained in primary antibody in blocking buffer overnight 4°C. The next day, cells were washed 3x in PBS and placed in secondary antibody 1:1000 in blocking buffer for 1hr room temp. Cells were washed 3x in PBS and stained with DAPI for 10min RT, washed once with PBS, then mounted in ProLong Gold antifade Mountant. Primary antibodies used for the immunofluorescence imaging: mouse anti-NCAM (Santa Cruz, SC-106 1:50), rab anti-Tau (Aligent/DAKO, A002401-2 1:200), rab anti-TUBB3 (Biolegend, 802001 1:2000), mouse anti-TUBB3 (Biolegend, 801202 1:2000), chicken anti-TUBB3 (Novus, NB100-1612 1:1000), mouse anti-tau (CP27) (generously provided by Dr. Peter Davies, 1:400), rabbit anti-MAP2 (Cell Signaling, #4542 1:200), rabbit anti-MAP2 (Millipore, AB5622 1:1000). The secondary antibodies were goat anti-mouse, -rabbit, or -chick IgG conjugated with Alexa-488, Alexa-594, or Alexa-647 (Invitrogen).

Immunostained images were taken using a Leica SP5X white light laser confocal system with Leica Application Suite (LAS) Advanced Fluorescence 2.7.3.9723. All antibodies were validated for functionality through negative control screening of fibroblasts.

Quantitative PCR (qPCR)

Total RNA was extracted from miNs using TRIzol (Invitrogen, USA) following manufacturer protocol. Reverse-transcription was performed with 150-200ng of RNA with SuperScript IV First Strand Synthesis SuperMix (Invitrogen, USA). qPCR assay was run with SYBR Green PCR Master Mix and plate was run and analyzed on StepOnePlus Real-Time PCR System (AB Applied Biosystems, Germany). Each sample was run in triplicate and the mean of each sample is represented as a single data point.

Semi-quantitative PCR (sq-PCR)

Semi-quantitative PCR was performed to quantify the ratio of 3R:4R mRNA. To perform sqPCR, cDNA was generated from RNA (SuperScript IV Reverse Transcriptase, ThermoFisher 18090010) then amplified using primers (Choi et al., 2014) flanking exon 10 (forward 5'-AAGTCGCCGTCTCCGCCAAG-3'; reverse 5'GTCCAGGGACCCAATCTCGA-3'). The PCR product was then run on a 2% agarose gel with 381bp and 288bp fragments indicating 4R and 3R, respectively. Ratios were then calculated as previously described (Antiabong et al., 2016).

Lysate Preparation for mass spectrometry analysis

MiNs were collected on PID 30. iPSC-Ns were collected after six weeks. Both were collected in the same manner. Briefly, media was removed and cells were washed once with DPBS. Fresh DPBS was added to the wells and cells were scraped off. Resuspended cells were pelleted at 1000g for 5min at RT, supernatant was removed, and pellets were frozen at -80°C until use.

Three different lots of Human Primary Neurons were purchased from ScienCell and plated according to manufacturer's instructions. Cells were cultured in Neuronal Medium (ScienCell #1521) for one week and collected same as the miNs and iPSC-Ns.

Adult brain frozen tissues were prepared as previously described (Horie et al., 2020).

Immunoprecipitation and mass spectrometry of tau isoforms

Mass spectrometry analyses of tau proteins were performed as previously described with some modifications (Barthélemy et al., 2020a; Barthélemy et al., 2020b; Horie et al., 2020; Sato et al., 2018). Briefly, cells and brain homogenates were diluted with PBS and 2% human serum

albumin (Sigma D4197) respectively, and lysed with final concentration of 0.5% NP-40 and 2.5mM guanidine. Tau protein was immunoprecipitated with mouse anti-Tau (Tau1) (provided by Dr. Nicholas Kanaan, 1.125 μ g/sample), and mouse anti-human tau (HJ8.5) (provided by Dr. David Holtzman, 2.25 μ g/sample), digested with trypsin, oxidized, desalting and subjected to nano-Acquity LC and MS analyses using Orbitrap Eclipse Tribrid Mass Spectrometer (Thermo Scientific).

All samples were spiked with full length ^{15}N -labeled 2N4R recombinant tau as an internal standard and ratios of isoforms were calculated by using 2N and 4R isoform-specific peptides compared to constitutive peptides (all peptide numbers are in reference to 2N4R isoform). For 2N, the 2N-specific tryptic peptide 68-87 was divided by the common peptide 151-155 to obtain percentage of 2N. 1N isoform percentage was calculated by dividing a shared 1N/2N peptide, 45-67, by the common peptide 151-155, to obtain the cumulative percentage of 1N+2N isoforms. The previously calculated 2N percentage was subtracted from this shared 1N/2N percentage to calculate the 1N percentage. 0N percentage was calculated by subtracting both 1N and 2N percentages from 100. Percent 4R was calculated three ways by dividing each of the R2 region, 4R-specific peptides, 275-280, 282-290, and 299-317, by the constitutive adjacent R1 peptide, 260-267. 3R was calculated by subtracting the 4R percentage from 100.

Immunoblot analysis

Media was aspirated from wells, cells were washed with DPBS, and lysed in the plate with RIPA (Sigma #R0278) supplemented with cOmplete Mini Protease Inhibitor Cocktail (Roche #11836153001). Lysate was collected and centrifuged at 13,000g for 10 minutes at 4°C. BCA protein assay determined protein content and samples were normalized with RIPA/protease inhibitor. Samples were treated with Lambda Phosphatase (NEB #P0753L) for 3 hours at 30°C. LDS NuPAGE sample buffer with 5% β -mercaptoethanol was added and samples were heated to 95°C for 3 minutes then loaded onto a 4-20% Tris-glycine gel (Novex XP04205BOX) or NuPAGE 8% 20-well Midi gel (Invitrogen WG1002), with tau protein ladder made from individual tau protein isoforms (SignalChem T02-54N, T03-54N, T04-54N, T05-54N, T06-54N, T07-54N) or Tau Peptide Ladder (rPeptide T-1007-2). After running, the gel was transferred onto either 0.45 μm PVDF membrane for 2hr at 400mA or 0.45 μm Nitrocellulose for 2hr at 200mV. Membrane was both blocked and treated with primary antibodies in either 5% Milk/TBS/0.1% Tween20 or just TBS/0.1% Tween20 overnight at 4°C: rabbit anti-Tau antibody (Aligent/DAKO, A002401-2 1:1000-10,000). The next day, nitrocellulose was washed 3 times with TBST, then treated with peroxidase-conjugated goat anti-rabbit secondary antibodies in 5% Milk/TBS/0.1% Tween 20 for up to 3hrs at RT. Membrane was washed 3 times with TBS/0.1% Tween20 and developed with the ECL system (Thermo Scientific, #34076) and imaged on a BioRad GelDoc imager (BioRad) or Sapphire Imager (Azure Biosystems).

SiRNA treatment of miNs

MiNs were replated, as per the above protocol, at PID 5 on 24 well Sensoplate (Greiner, 662892) previously coated with poly-ornithine, laminin, and fibronectin.

At PID 18, cells were treated with 1uM of Dharmacon™ Accell™ siRNAs: Accell Human MAPT (4137) siRNA-SMARTpool (E-012488-00-0050) and Accell Non-targeting Pool (D-001910-10-05). Treatment was left on until PID 26 when cells were fixed with 100% methanol to extract soluble proteins, as described previously(Guo *et al.*, 2016; Katsikoudi *et al.*, 2020). In brief, the growth media was completely aspirated, and cells were washed twice with 200 μL /well of DPBS. Ice-cold 100% methanol was added 200 μL /well for 15 minutes at room temperature. Subsequently, the cells were washed three times with 200 μL /well of DPBS, with the final wash

being left on for storage. Plates were kept at 4°C until immunocytochemistry (ICC) was performed.

Immunocytochemistry, imaging and analysis

Fixed cells in DPBS had the liquid tipped off, and the cells were blocked with 200 µL/well of Intercept Blocking Buffer (LI-COR) containing 0.1% Triton for one hour at room temperature. The primary antibodies CP-27, kindly provided by Peter Davies, and MAP2 (Millipore, AB5622) were prepared in Blocking Buffer at 1:1000 and incubated overnight at 4°C with gentle agitation.

On the following day, the primary antibody was tipped off, and the cells were washed three times with 200 µL/well of DPBS. The secondary antibodies Goat anti-mouse IgG2b 647 Alexa Flour-conjugated antibody (A-21242) and Goat anti-rabbit 488 Alexa Flour-conjugated antibody (A-11008), as well as Hoechst 33342 (Invitrogen) were prepared at 1:1000 in Blocking Buffer and left for 1 hour at room temperature.

The plates were then washed three times with 200 µL/well of DPBS, before being left in DPBS at 4°C until high-content imaging using the Opera Phenix (Perkin Elmer). Images were taken using a 20X water objective, with 75 fields of view per well, and a Z-stack of 6 slices. The images were analysed using Perkin Elmer software Harmony as previously described (Katsikoudi *et al.*, 2020). Briefly, stacks of each image were maximum projected and filtered using the sliding parabola to smoothen the background and get rid of the fluorescent noise. Subsequently, machine learning was used to define the tau positive area used as region in which the software was trained to identify the CP-27 positive threads. Total nuclei were also detected and analyzed. At the end of the analysis results were exported in an Excel file divided by object (total nuclei and CP-27 count) and well. The final readout was “CP-27 inclusion count normalized to the total nuclei count”. Data was plotted in GraphPad.

Biosensor cell culture methods

MiNs were harvested on PID 26 in 50 mM Tris-HCl, pH 7.5 150 mM NaCl. The lysates were sonicated for 4.5 minutes at 50% amplitude (QSonica, Q800R3 Sonicator). BCA assay was used determine protein concentration of protein. HEK biosensor Tau RD-CFP/YFP cell line, kindly provided by Dr. Marc Diamond (Furman *et al.*, 2015), were cultured in 10 cm dish in DMEM (+Pyruvate, + D-glucose/D-glutamine) (Thermofisher) with 10%FBS and 1% Pen-Strep. The day before the seeding experiment, cells were replated in a 96-well plate at a density of 40,000 cells/well in 130uL of media and left adhere over-night. The following day, cells were seeded with miN lysates; the seeding mixes were made by combining 17µg of total protein lysate per well to 3.75µL of Opti-MEM (Gibco) and 1.25uL Lipofectamine 2000 (Invitrogen) for a total volume of 20 µL per well. Liposome preparations were incubated at room temperature for 30 min before adding to cells, and each condition was done in triplicate. Cells were incubated with seeding mixes for 72 h before the analysis.

FRET Flow Cytometry

After 72 h from the seeding, cells were washed in PBS (Gibco), harvested with 0.25% trypsin and fixed in 4% paraformaldehyde for 10 min, then resuspended in flow cytometry buffer (1 mM EDTA in PBS). The BD LSRFortessa™ Flow Cytometer was used to perform FRET flow cytometry as previously described (Furman *et al.*, 2015). Briefly, to measure CFP and FRET, cells were excited with the 405 nm laser, and to measure YFP cells were excited with a 488 nm laser. Fluorescence was captured with a 405/50 nm, 525/50 nm and 525/50 nm filters respectively.

To quantify FRET, a gating strategy similar to that previously described was used(Furman *et al.*, 2015): first the CFP bleed-through into the YFP and FRET channels was compensated, and cells were gated in order to exclude YFP-positive only cells emitting in the FRET signal. A bivariate plot of FRET vs. CFP was made to assess the number of FRET-positive cells. The percentage of FRET (i.e., the number of FRET-positive cells per total cell count) and the Integrated FRET density (i.e. product of percent positivity and median fluorescence intensity) were used for the analyses. For each experiment, 20,000 cells per replicate were analyzed and each condition was analyzed in triplicate. Data analysis was performed using FCS Express 7 Research software (De Novo Software).

Supplemental Information

Figures

Figure S1, related to Figure 1 and 3

Figure S2, related to Figure 4

REFERENCES

- Abernathy, D.G., Kim, W.K., McCoy, M.J., Lake, A.M., Ouwenga, R., Lee, S.W., Xing, X., Li, D., Lee, H.J., Heuckeroth, R.O., et al. (2017). MicroRNAs Induce a Permissive Chromatin Environment that Enables Neuronal Subtype-Specific Reprogramming of Adult Human Fibroblasts. *Cell Stem Cell* 21, 332-348.e339. 10.1016/j.stem.2017.08.002.
- Abernathy, D.G., and Yoo, A.S. (2015). MicroRNA-dependent genetic networks during neural development. *Cell Tissue Res.* 359, 179-185. 10.1007/s00441-014-1899-4.
- Antiabong, J.F., Ngoepe, M.G., and Abechi, A.S. (2016). Semi-quantitative digital analysis of polymerase chain reaction-electrophoresis gel: Potential applications in low-income veterinary laboratories. *Vet World* 9, 935-939. 10.14202/vetworld.2016.935-939.
- Barthélemy, N.R., Bateman, R.J., Hirtz, C., Marin, P., Becher, F., Sato, C., Gabelle, A., and Lehmann, S. (2020a). Cerebrospinal fluid phospho-tau T217 outperforms T181 as a biomarker for the differential diagnosis of Alzheimer's disease and PET amyloid-positive patient identification. *Alzheimer's Research & Therapy* 12. 10.1186/s13195-020-00596-4.
- Barthélemy, N.R., Li, Y., Joseph-Mathurin, N., Gordon, B.A., Hassenstab, J., Benzinger, T.L.S., Buckles, V., Fagan, A.M., Perrin, R.J., Goate, A.M., et al. (2020b). A soluble phosphorylated tau signature links tau, amyloid and the evolution of stages of dominantly inherited Alzheimer's disease. *Nature Medicine* 26, 398-407. 10.1038/s41591-020-0781-z.
- Beevers, J.E., Lai, M.C., Collins, E., Booth, H.D.E., Zambon, F., Parkkinen, L., Vowles, J., Cowley, S.A., Wade-Martins, R., and Caffrey, T.M. (2017). MAPT Genetic Variation and Neuronal Maturity Alter Isoform Expression Affecting Axonal Transport in iPSC-Derived Dopamine Neurons. *Stem Cell Reports* 9, 587-599. 10.1016/j.stemcr.2017.06.005.
- Braak, H., and Del Tredici, K. (2010). Neurofibrillary Tangles. In *Encyclopedia of Movement Disorders*, K. Kompoliti, and L.V. Metman, eds. (Academic Press), pp. 265-269.
<https://doi.org/10.1016/B978-0-12-374105-9.00269-0>.

- Cates, K., Mccoy, M.J., Kwon, J.-S., Liu, Y., Abernathy, D.G., Zhang, B., Liu, S., Gontarz, P., Kim, W.K., Chen, S., et al. (2020). Deconstructing Stepwise Fate Conversion of Human Fibroblasts to Neurons by MicroRNAs. *Cell Stem Cell*. 10.1016/j.stem.2020.08.015.
- Cavaloc, Y., Popielarz, M., Fuchs, J.P., Gattoni, R., and Stévenin, J. (1994). Characterization and cloning of the human splicing factor 9G8: a novel 35 kDa factor of the serine/arginine protein family. *The EMBO Journal* 13, 2639-2649. 10.1002/j.1460-2075.1994.tb06554.x.
- Choi, S.H., Kim, Y.H., Hebisch, M., Sliwinski, C., Lee, S., D'Avanzo, C., Chen, H., Hooli, B., Asselin, C., Muffat, J., et al. (2014). A three-dimensional human neural cell culture model of Alzheimer's disease. *Nature* 515, 274-278. 10.1038/nature13800.
- Clavaguera, F., Bolmont, T., Crowther, R.A., Abramowski, D., Frank, S., Probst, A., Fraser, G., Stalder, A.K., Beibel, M., Staufenbiel, M., et al. (2009). Transmission and spreading of tauopathy in transgenic mouse brain. *Nature Cell Biology* 11, 909-913. 10.1038/ncb1901.
- Connell, J.W., Rodriguez-Martin, T., Gibb, G.M., Kahn, N.M., Grierson, A.J., Hanger, D.P., Revesz, T., Lantos, P.L., Anderton, B.H., and Gallo, J.M. (2005). Quantitative analysis of tau isoform transcripts in sporadic tauopathies. *Molecular Brain Research* 137, 104-109. 10.1016/j.molbrainres.2005.02.014.
- Ding, S., Shi, J., Qian, W., Iqbal, K., Grundke-Iqbali, I., Gong, C.-X., and Liu, F. (2012). Regulation of alternative splicing of tau exon 10 by 9G8 and Dyk1A. *Neurobiology of Aging* 33, 1389-1399. 10.1016/j.neurobiolaging.2010.11.021.
- Duff, K., Knight, H., Refolo, L.M., Sanders, S., Yu, X., Picciano, M., Malester, B., Hutton, M., Adamson, J., Goedert, M., et al. (2000). Characterization of Pathology in Transgenic Mice Over-Expressing Human Genomic and cDNA Tau Transgenes. *Neurobiology of Disease* 7, 87-98. 10.1006/nbdi.1999.0279.
- Ehrlich, M., Hallmann, A.-L., Reinhardt, P., Araúzo-Bravo, J., Marcos, Korr, S., Röpke, A., Psathaki, E., Olympia, Ehling, P., Meuth, G., Sven, Oblak, L., Adrian, et al. (2015). Distinct Neurodegenerative Changes in an Induced Pluripotent Stem Cell Model of Frontotemporal Dementia Linked to Mutant TAU Protein. *Stem Cell Reports* 5, 83-96. 10.1016/j.stemcr.2015.06.001.
- Frost, B., Jacks, R.L., and Diamond, M.I. (2009). Propagation of Tau Misfolding from the Outside to the Inside of a Cell. *Journal of Biological Chemistry* 284, 12845-12852. 10.1074/jbc.m808759200.
- Furman, J.L., Holmes, B.B., and Diamond, M.I. (2015). Sensitive Detection of Proteopathic Seeding Activity with FRET Flow Cytometry. *Journal of Visualized Experiments*. 10.3791/53205.
- Gao, Y.-L., Wang, N., Sun, F.-R., Cao, X.-P., Zhang, W., and Yu, J.-T. (2018). Tau in neurodegenerative disease. *Ann Transl Med* 6. 10.21037/atm.2018.04.23.
- Ghetti, B., Oblak, A.L., Boeve, B.F., Johnson, K.A., Dickerson, B.C., and Goedert, M. (2015). Invited review: Frontotemporal dementia caused by microtubule-associated protein tau gene (MAPT) mutations: a chameleon for neuropathology and neuroimaging: MAPT mutations and FTD. *Neuropathology and Applied Neurobiology* 41, 24-46. 10.1111/nan.12213.
- Goedert, M., and Jakes, R. (1990). Expression of separate isoforms of human tau protein: correlation with the tau pattern in brain and effects on tubulin polymerization. *The EMBO Journal* 9, 4225-4230. 10.1002/j.1460-2075.1990.tb07870.x.

Goedert, M., Spillantini, M.G., Jakes, R., Rutherford, D., and Crowther, R.A. (1989a). Multiple isoforms of human microtubule-associated protein tau: sequences and localization in neurofibrillary tangles of Alzheimer's disease. *Neuron* 3, 519-526. 10.1016/0896-6273(89)90210-9.

Goedert, M., Spillantini, M.G., Potier, M.C., Ulrich, J., and Crowther, R.A. (1989b). Cloning and sequencing of the cDNA encoding an isoform of microtubule-associated protein tau containing four tandem repeats: differential expression of tau protein mRNAs in human brain. *The EMBO Journal* 8, 393-399.

Götz, J., Halliday, G., and Nisbet, R.M. (2019). Molecular Pathogenesis of the Tauopathies. *Annual Review of Pathology: Mechanisms of Disease* 14, 239-261. 10.1146/annurev-pathmechdis-012418-012936.

Grover, A., Houlden, H., Baker, M., Adamson, J., Lewis, J., Prihar, G., Pickering-Brown, S., Duff, K., and Hutton, M. (1999). 5' splice site mutations in tau associated with the inherited dementia FTDP-17 affect a stem-loop structure that regulates alternative splicing of exon 10. *The Journal of Biological Chemistry* 274, 15134-15143.

Guo, J.L., and Lee, V.M.-Y. (2011). Seeding of Normal Tau by Pathological Tau Conformers Drives Pathogenesis of Alzheimer-like Tangles. *Journal of Biological Chemistry* 286, 15317-15331. 10.1074/jbc.m110.209296.

Guo, J.L., Narasimhan, S., Changolkar, L., He, Z., Stieber, A., Zhang, B., Gathagan, R.J., Iba, M., McBride, J.D., Trojanowski, J.Q., and Lee, V.M.Y. (2016). Unique pathological tau conformers from Alzheimer's brains transmit tau pathology in nontransgenic mice. *Journal of Experimental Medicine* 213, 2635-2654. 10.1084/jem.20160833.

Hefti, M.M., Farrell, K., Kim, S., Bowles, K.R., Fowkes, M.E., Raj, T., and Crary, J.F. (2018). High-resolution temporal and regional mapping of MAPT expression and splicing in human brain development. *PLOS ONE* 13, e0195771. 10.1371/journal.pone.0195771.

Himmler, A., Drechsel, D., Kirschner, M.W., and Martin, D.W. (1989). Tau consists of a set of proteins with repeated C-terminal microtubule-binding domains and variable N-terminal domains. *Molecular and Cellular Biology* 9, 1381-1388.

Holmes, B.B., Furman, J.L., Mahan, T.E., Yamasaki, T.R., Mirbaha, H., Eades, W.C., Belaygorod, L., Cairns, N.J., Holtzman, D.M., and Diamond, M.I. (2014). Proteopathic tau seeding predicts tauopathy in vivo. *Proceedings of the National Academy of Sciences of the United States of America* 111, E4376-E4385. 10.1073/pnas.1411649111.

Horie, K., Barthélémy, N.R., Mallipeddi, N., Li, Y., Franklin, E.E., Perrin, R.J., Bateman, R.J., and Sato, C. (2020). Regional correlation of biochemical measures of amyloid and tau phosphorylation in the brain. *Acta Neuropathologica Communications* 8. 10.1186/s40478-020-01019-z.

Huh, C.J., Zhang, B., Victor, M.B., Dahiya, S., Batista, L.F., Horvath, S., and Yoo, A.S. (2016). Maintenance of age in human neurons generated by microRNA-based neuronal conversion of fibroblasts. *eLife* 5. 10.7554/eLife.18648.

Hutton, M., Lendon, C.L., Rizzu, P., Baker, M., Froelich, S., Houlden, H., Pickering-Brown, S., Chakraverty, S., Isaacs, A., Grover, A., et al. (1998). Association of missense and 5'-splice-site mutations in tau with the inherited dementia FTDP-17. *Nature* 393, 702-705. 10.1038/31508.

Ishigaki, S., Fujioka, Y., Okada, Y., Riku, Y., Udagawa, T., Honda, D., Yokoi, S., Endo, K., Ikenaka, K., Takagi, S., et al. (2017). Altered Tau Isoform Ratio Caused by Loss of FUS and SFPQ Function Leads to FTLD-like Phenotypes. *Cell Reports* 18, 1118-1131. 10.1016/j.celrep.2017.01.013.

Jiang, S., Wen, N., Li, Z., Dube, U., Del Aguila, J., Budde, J., Martinez, R., Hsu, S., Fernandez, M.V., Cairns, N.J., et al. (2018). Integrative system biology analyses of CRISPR-edited iPSC-derived neurons and human brains reveal deficiencies of presynaptic signaling in FTLD and PSP. *Transl Psychiatry* 8. 10.1038/s41398-018-0319-z.

Karch, C.M., Kao, A.W., Karydas, A., Onanuga, K., Martinez, R., Argouarch, A., Wang, C., Huang, C., Sohn, P.D., Bowles, K.R., et al. (2019). A Comprehensive Resource for Induced Pluripotent Stem Cells from Patients with Primary Tauopathies. *Stem Cell Reports* 13, 939-955. 10.1016/j.stemcr.2019.09.006.

Katsikoudi, A., Ficulle, E., Cavallini, A., Sharman, G., Guyot, A., Zagnoni, M., Eastwood, B.J., Hutton, M., and Bose, S. (2020). Quantitative propagation of assembled human Tau from Alzheimer's disease brain in microfluidic neuronal cultures. *Journal of Biological Chemistry* 295, 13079-13093. 10.1074/jbc.ra120.013325.

Kosik, K.S., Orecchio, L.D., Bakalis, S., and Neve, R.L. (1989). Developmentally regulated expression of specific tau sequences. *Neuron* 2, 1389-1397. 10.1016/0896-6273(89)90077-9.

Lapasset, L., Milhavet, O., Prieur, A., Besnard, E., Babled, A., Aït-Hamou, N., Leschik, J., Pellestor, F., Ramirez, J.-M., De Vos, J., et al. (2011). Rejuvenating senescent and centenarian human cells by reprogramming through the pluripotent state. *Genes & Development* 25, 2248-2253. 10.1101/gad.173922.111.

Li, X., Zuo, X., Jing, J., Ma, Y., Wang, J., Liu, D., Zhu, J., Du, X., Xiong, L., Du, Y., et al. (2015). Small-Molecule-Driven Direct Reprogramming of Mouse Fibroblasts into Functional Neurons. *Cell Stem Cell* 17, 195-203. 10.1016/j.stem.2015.06.003.

Lim, L.P., Lau, N.C., Garrett-Engele, P., Grimson, A., Schelter, J.M., Castle, J., Bartel, D.P., Linsley, P.S., and Johnson, J.M. (2005). Microarray analysis shows that some microRNAs downregulate large numbers of target mRNAs. *Nature* 433, 769-773. 10.1038/nature03315.

Liu, L., Drouet, V., Wu, J.W., Witter, M.P., Small, S.A., Clelland, C., and Duff, K. (2012). Trans-Synaptic Spread of Tau Pathology In Vivo. *PLOS ONE* 7, e31302. 10.1371/journal.pone.0031302.

Lu, Y.-L., and Yoo, A.S. (2018). Mechanistic Insights Into MicroRNA-Induced Neuronal Reprogramming of Human Adult Fibroblasts. *Frontiers in Neuroscience* 12, 522. 10.3389/fnins.2018.00522.

Marone, M., Mozzetti, S., De Ritis, D., Pierelli, L., and Scambia, G. (2001). Semiquantitative RT-PCR analysis to assess the expression levels of multiple transcripts from the same sample. *Biol Proced Online* 3, 19-25. 10.1251/bpo20.

Mertens, J., Herdy, J.R., Traxler, L., Schafer, S.T., Schlachetzki, J.C.M., Böhnke, L., Reid, D.A., Lee, H., Zangwill, D., Fernandes, D.P., et al. (2021). Age-dependent instability of mature neuronal fate in induced neurons from Alzheimer's patients. *Cell Stem Cell*. 10.1016/j.stem.2021.04.004.

Nuclear Reprogramming: Methods and Protocols. (2021). 1 Edition (Springer Science+Business Media, LLC, part of Springer Nature). 10.1007/978-1-0716-1084-8.

Patterson, M., Chan, D.N., Ha, I., Case, D., Cui, Y., Van Handel, B., Mikkola, H.K., and Lowry, W.E. (2012). Defining the nature of human pluripotent stem cell progeny. *Cell Res.* 22, 178-193. 10.1038/cr.2011.133.

Richner, M., Victor, M.B., Liu, Y., Abernathy, D., and Yoo, A.S. (2015). MicroRNA-based conversion of human fibroblasts into striatal medium spiny neurons. *Nat Protoc* 10, 1543-1555. 10.1038/nprot.2015.102.

Safety, Tolerability and Pharmacokinetics of Multiple Ascending Doses of NIO752 in Progressive Supranuclear Palsy. <https://ClinicalTrials.gov/show/NCT04539041>.

Sato, C., Barthélémy, N.R., Mawuenyega, K.G., Patterson, B.W., Gordon, B.A., Jockel-Balsarotti, J., Sullivan, M., Crisp, M.J., Kasten, T., Kirmess, K.M., et al. (2018). Tau Kinetics in Neurons and the Human Central Nervous System. *Neuron* 97, 1284-1298.e1287. 10.1016/j.neuron.2018.02.015.

Siahaan, V., Krattenmacher, J., Hyman, A.A., Diez, S., Hernández-Vega, A., Lansky, Z., and Braun, M. (2019). Kinetically distinct phases of tau on microtubules regulate kinesin motors and severing enzymes. *Nature Cell Biology* 21, 1086-1092. 10.1038/s41556-019-0374-6.

Sposito, T., Preza, E., Mahoney, C.J., Setó-Salvia, N., Ryan, N.S., Morris, H.R., Arber, C., Devine, M.J., Houlden, H., Warner, T.T., et al. (2015). Developmental regulation of tau splicing is disrupted in stem cell-derived neurons from frontotemporal dementia patients with the 10 + 16 splice-site mutation in MAPT. *Human Molecular Genetics* 24, 5260-5269. 10.1093/hmg/ddv246.

Tan, R., Lam, A.J., Tan, T., Han, J., Nowakowski, D.W., Vershinin, M., Simó, S., Ori-McKenney, K.M., and McKenney, R.J. (2019). Microtubules gate tau condensation to spatially regulate microtubule functions. *Nature Cell Biology* 21, 1078-1085. 10.1038/s41556-019-0375-5.

Tan, S.-L., Ohtsuka, T., González, A., and Kageyama, R. (2012). MicroRNA9 regulates neural stem cell differentiation by controlling Hes1 expression dynamics in the developing brain. *Genes to Cells* 17, 952-961. 10.1111/gtc.12009.

Verheyen, A., Diels, A., Dijkmans, J., Oyelami, T., Meneghelli, G., Mertens, L., Versweyveld, S., Borgers, M., Buist, A., Peeters, P., and Cik, M. (2015). Using Human iPSC-Derived Neurons to Model TAU Aggregation. *PLOS ONE* 10, e0146127. 10.1371/journal.pone.0146127.

Verheyen, A., Diels, A., Reumers, J., Van Hoorde, K., Van den Wyngaert, I., van Outryve d'Ydewalle, C., De Bondt, A., Kuijlaars, J., De Muynck, L., De Hoogt, R., et al. (2018). Genetically Engineered iPSC-Derived FTDP-17 MAPT Neurons Display Mutation-Specific Neurodegenerative and Neurodevelopmental Phenotypes. *Stem Cell Reports* 11, 363-379. 10.1016/j.stemcr.2018.06.022.

Victor, M.B., Richner, M., Hermanstyne, T.O., Ransdell, J.L., Sobieski, C., Deng, P.-Y., Klyachko, V.A., Nerbonne, J.M., and Yoo, A.S. (2014). Generation of human striatal neurons by microRNA-dependent direct conversion of fibroblasts. *Neuron* 84, 311-323. 10.1016/j.neuron.2014.10.016.

Victor, M.B., Richner, M., Olsen, H.E., Lee, S.W., Monteys, A.M., Ma, C., Huh, C.J., Zhang, B., Davidson, B.L., Yang, X.W., and Yoo, A.S. (2018). Striatal neurons directly converted from Huntington's disease patient fibroblasts recapitulate age-associated disease phenotypes. *Nature Neuroscience* 21, 341-352. 10.1038/s41593-018-0075-7.

Wang, J., Gao, Q.-S., Wang, Y., Lafyatis, R., Stamm, S., and Andreadis, A. (2004). Tau exon 10, whose missplicing causes frontotemporal dementia, is regulated by an intricate interplay of

cis elements and trans factors. *Journal of Neurochemistry* 88, 1078-1090. 10.1046/j.1471-4159.2003.02232.x.

Yoo, A.S., Staahl, B.T., Chen, L., and Crabtree, G.R. (2009). MicroRNA-mediated switching of chromatin-remodelling complexes in neural development. *Nature* 460, 642-646. 10.1038/nature08139.

Yoo, A.S., Sun, A.X., Li, L., Shcheglovitov, A., Portmann, T., Li, Y., Lee-Messer, C., Dolmetsch, R.E., Tsien, R.W., and Crabtree, G.R. (2011). MicroRNA-mediated conversion of human fibroblasts to neurons. *Nature* 476, 228-231. 10.1038/nature10323.

Zhao, C., Sun, G., Li, S., and Shi, Y. (2009). A feedback regulatory loop involving microRNA-9 and nuclear receptor TLX in neural stem cell fate determination. *Nature Structural & Molecular Biology* 16, 365-371. 10.1038/nsmb.1576.

Key Resources Table

REAGENT or RESOURCE	SOURCE	IDENTIFIER
Antibodies		
Rabbit polyclonal anti-MAP2	Cell Signaling Technology	Cat# 4542S; RRID: AB_10693782
Rabbit polyclonal anti-MAP2	Millipore	Cat# AB5622; RRID: AB_91939
Rabbit polyclonal anti-Tau	Alight/Dako	Cat# 002401-2; RRID: AB_10013724
Mouse monoclonal anti-TUBB3	BioLegend	Cat# 801202; RRID: AB_10063408
Rabbit polyclonal anti-TUBB3	BioLegend	Cat# 802001; RRID: AB_2564645
Chicken polyclonal anti-TUBB3	Novus	Cat# NB100-1612, RRID: AB_10000548
Mouse monoclonal anti-Tau (CP-27)	Peter Davies, Albert Einstein College of Medicine	Cat# CP-27; RRID: AB_2716722
Mouse monoclonal anti-Tau (Tau1)	Nicholas M. Kanaan, Michigan State University	Cat# Tau1; RRID: AB_2721197
Mouse monoclonal anti-Tau (HJ8.5)	David Holtzman, Washington University in St. Louis	Cat# HJ8.5; RRID: AB_2721237
Mouse monoclonal anti-NCAM1	Santa Cruz Biotechnology	Cat#SC-106; RRID: AB_627128
Chemicals, Peptides, and Recombinant Proteins		
Fetal bovine serum (FBS), qualified, US Department of Agriculture (USDA)-approved regions	Life Technologies	Cat# 10437028
Polybrene	Sigma-Aldrich	Cat# H9268
Neuronal Media	ScienCell Research Laboratories	Cat# 1521
Doxycycline hyclate (Dox)	Sigma-Aldrich	Cat# D9891
Poly-L-ornithine solution	Sigma-Aldrich	Cat# P4957
Laminin	Sigma-Aldrich	Cat# L2020
Fibronectin	Sigma-Aldrich	Cat# F4759
Valproic acid (VPA), sodium salt	Sigma-Aldrich	Cat# 676380
Dibutyryl-cAMP sodium salt	Sigma-Aldrich	Cat# D0627
Retinoic acid (RA)	Sigma-Aldrich	Cat# R2625
Neurotrophin-3 (NT-3)	PeproTech	Cat# 450-03
Brain-derived neurotrophic factor (BDNF)	PeproTech	Cat# 450-02
Ciliary Neurotrophic factor (CNTF)	PeproTech	Cat# 450-13
Glial-derived Neurotrophic Factor (GDNF)	PeproTech	Cat# 450-10
RevitaCell Supplement	Thermo Fisher Scientific	Cat# A2644501
ISX-9	StemCell Technologies	Cat# 73202
DAPT	Millipore Sigma	Cat# D5942
Critical Commercial Assays		
Go Taq DNA Polymerase	Promega	Cat# M3001
Deposited Data		
none		
Experimental Models: Cell Lines		
Fibroblasts used for reprogramming, see Table S1		

Fetal-aged products, see Table S2		
Adult human brain samples, see Table S3		
Lenti-X 293LE cell line	Clontech	Cat# 632180
Oligonucleotides		
Primers used for qPCR, see Table S4	This paper	N/A
Primers used for sqPCR, see Table S5	This paper	N/A
Recombinant DNA		
pMD2.G	Addgene	12259
psPAX2	Addgene	12260
rtTA-N144	Addgene	66810
pT-BCL-9/9*-124	Addgene	60857
MYT1L-N174	Addgene	66809
Software and Algorithms		
ImageJ	Schneider et al., 2012	https://imagej.nih.gov/ij/
LAS X	Leica Microsystems	https://www.leica-microsystems.com/products/microscope-software/p/leica-las-xs/
Harmony v4.9	Perkin Elmer	https://www.perkinelmer.com/product/harmony-4-8-office-hh17000001
Graphpad Prism 9	GraphPad Software Inc	http://www.graphpad.com/
FCS Express 7 Research software	De Novo Software	https://denovosoftware.com/
Xcaliber Software	Thermo Fisher Scientific	https://www.thermofisher.com/order/catalog/product/OPTON-30965#/OPTON-30965
Skyline	MacCoss Lab Software	https://skyline.ms/project/home/software/Skyline/begin.view

Table**Table S1, related to STAR Methods section: Fibroblast cell lines used.** List of fibroblast cell lines used.

Line	ID	Age	Sex	MAPT Mutation	Experiments
AG04148	Ctrl 1	56	M	None	ICC, sqPCR, MS, Insoluble, Biosensor
AG08260	Ctrl 2	61	M	None	ICC, sqPCR, MS
AG08379	Ctrl 3	60	F	None	ICC, sqPCR, MS, WB, Insoluble, Biosensor
AG13369	Ctrl 4	68	M	None	ICC, sqPCR, MS, Insoluble, Biosensor
UCL455	IVS10+16 1	53	M	IVS10+16 C>T	ICC, sqPCR, MS, Insoluble, Biosensor
UCL457	IVS10+16 2	52	M	IVS10+16 C>T	ICC, sqPCR, MS, Insoluble, Biosensor
UCL497	IVS10+16 3	54	F	IVS10+16 C>T	ICC, sqPCR, MS, WB, Insoluble, Biosensor
ES-046	IVS10+16 4	57	M	IVS10+16 C>T	ICC, sqPCR, MS, Insoluble, Biosensor

Table S2, related to STAR Methods section: Fetal-aged products used. List of fetal aged products used.

Product ID	Lot #	ID	Experiments
1F01-50	1333	FBrain 1	sqPCR, MS, RNAseq
1520	29207	FPN 1	sqPCR, MS
1520	28630	FPN 2	sqPCR, MS
1520	29390	FPN 3	sqPCR, MS
BX-0300	200107	iPSC-CN 1	RNAseq, sqPCR
1526	2219	FNL 1	WB

Table S3, related to STAR Methods section: Adult human brain samples. List of adult human brain products used.

Product ID	Lot #	ID	Age	Sex	Experiments
R1234035-50	C.210018	ABrain 1	29yr	M	RNAseq, sqPCR
R1234035-50	B.210080	ABrain 2	66yr	M	sqPCR
R1234035-50	B.811107	ABrain 3	78yr	F	sqPCR
NB820-59177	C.111050	ABrain 4	82yr	M	MS, WB
n/a	61732	ABrain 5	90	M	MS
n/a	65241	ABrain 6	80	M	MS
n/a	65318	ABrain 7	87	M	MS
n/a	84868	ABrain 8	72	M	MS

Table S4, related to STAR Methods section: qPCR Primers used. List of qPCR primer oligonucleotide sequences.

Primer	Sequence (5' > 3')
MAPT Forward	GGGGCTGATGGTAAACGAA
MAPT Reverse	CTCGCGATCCCCTGATTG
MAP2 Forward	CCCTTGAGAACACGACACA
MAP2 Reverse	TCTGTTAGCGGTGCTGAGGT
NEFL Forward	AGCTGGAGGACAAGCAGAAC
NEFL Reverse	TCCAAGCCATCTCACGTT
VGLUT1 Forward	ACGTGCGCAAGTTGATGA
VGLUT1 Reverse	TCACGTTGAACCCAGAGATG
TBR1 Forward	ACAATTTCTGACTCCAAGGAC

TBR1 Reverse	ACTGTGACGAAGCTCAGAGAC
MEF2C Forward	CCAGGCAGCAAGAATACGAT
MEF2C Reverse	TTGTTGAAATGGCTGATGGA
GRIN2C Forward	ACTTCTCCTTCAGCCCTGGT
GRIN2C Reverse	CTGCAGAGAGGCACTGTAGC
BRN2 Forward	GCTGTGGGAGAGAGAGGAGA
BRN2 Reverse	GCAGGCTGTAGTGGTAGACCG
NEUROD2 Forward	TGCTACTCCAAGACCGAGAAG
NEUROD2 Reverse	CACGTAGGACACTAGGTCTGG
GAPDH Forward	ATGTTCGTCATGGGTGTGAA
GAPDH Reverse	TGTGGTCATGAGTCCTCCA

Table S5, related to STAR Methods section: sqPCR Primers used. List of sqPCR primer oligonucleotide sequences.

Primer	Sequence (5' > 3')
MAPT Forward	AAGTCGCCGTCTTCCGCCAAG
MAPT Reverse	GTCCAGGGACCCAATCTTCGA
GAPDH Forward	ATGTTCGTCATGGGTGTGAA
GAPDH Reverse	TGTGGTCATGAGTCCTCCA

Figure 1

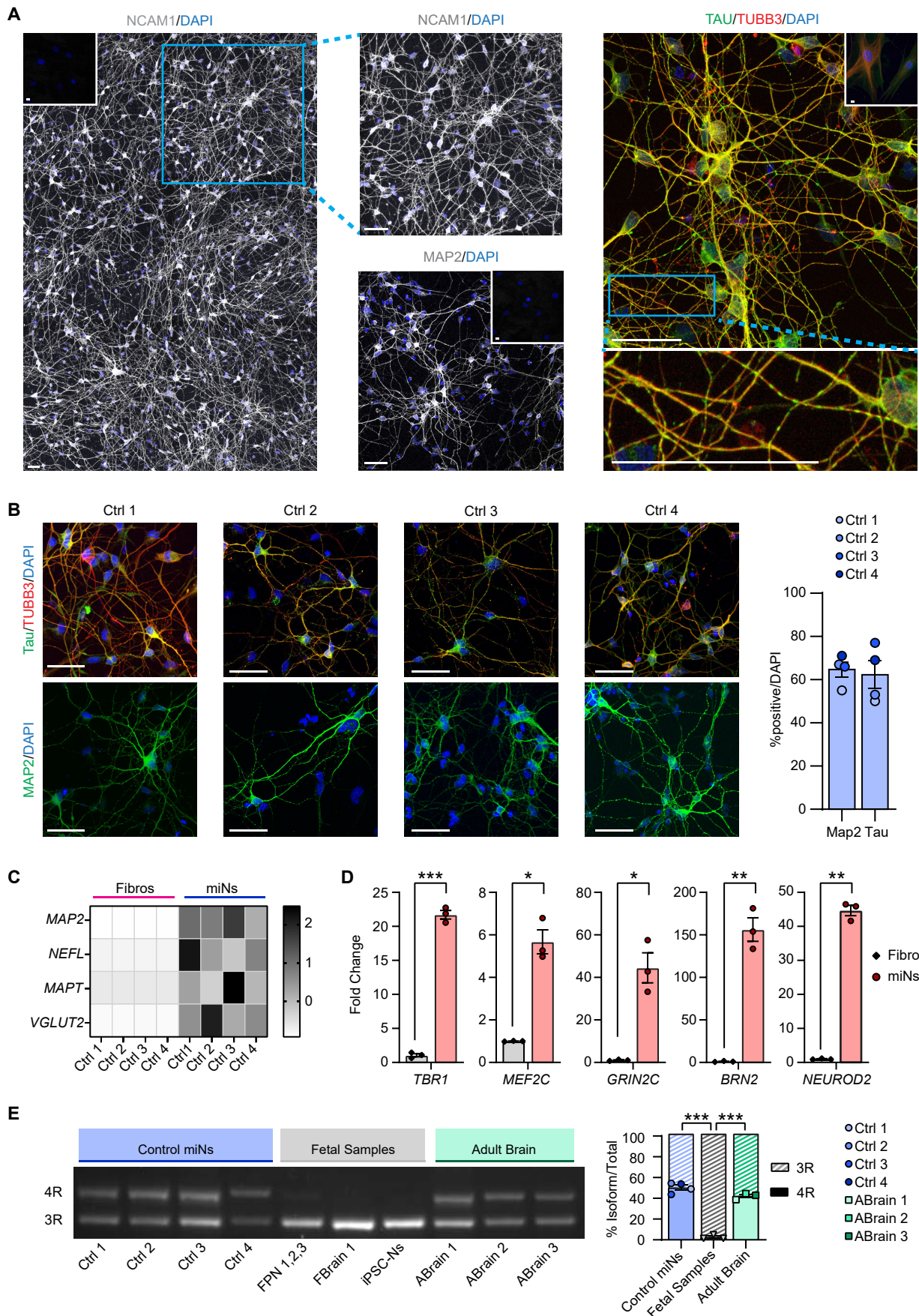


Figure 2

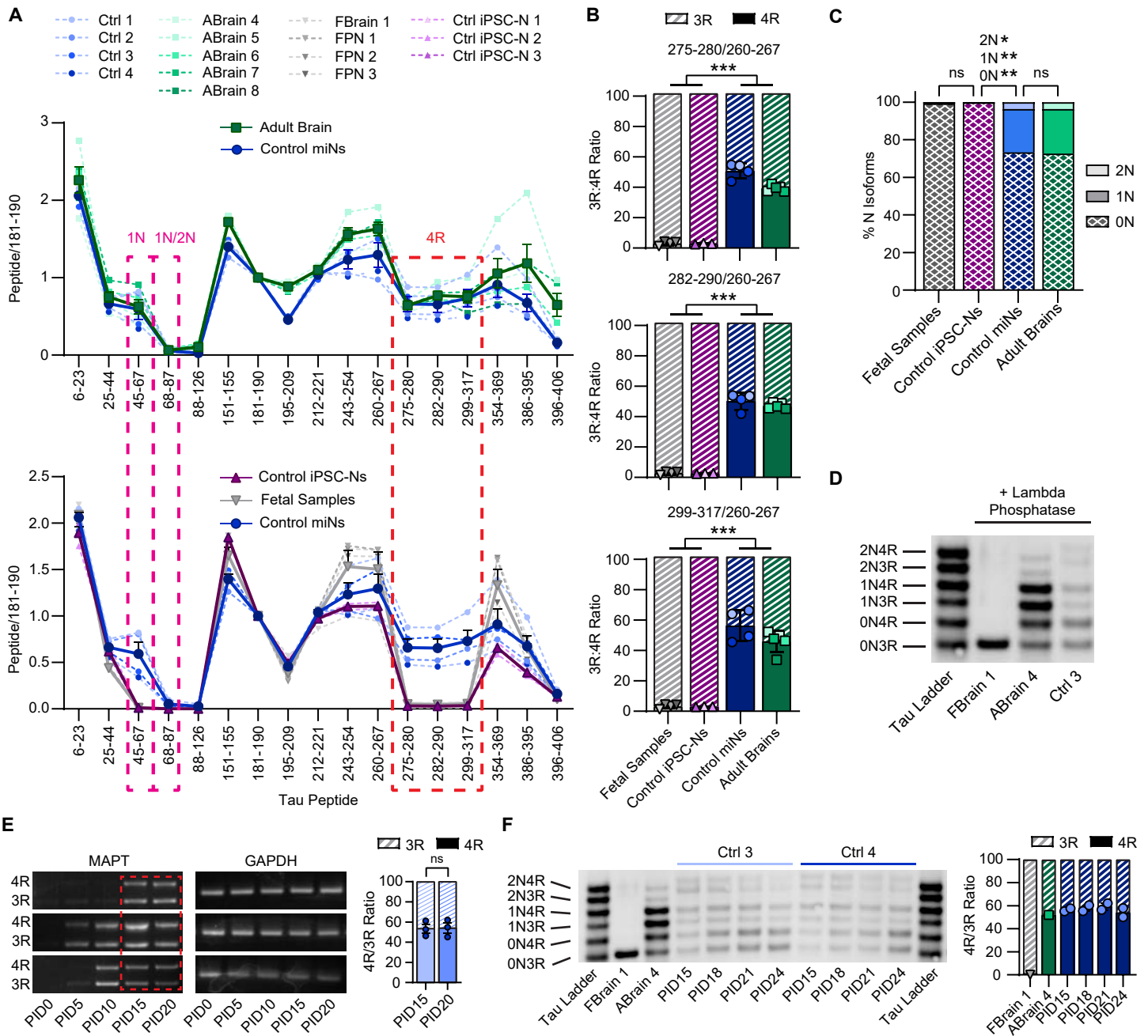


Figure 3

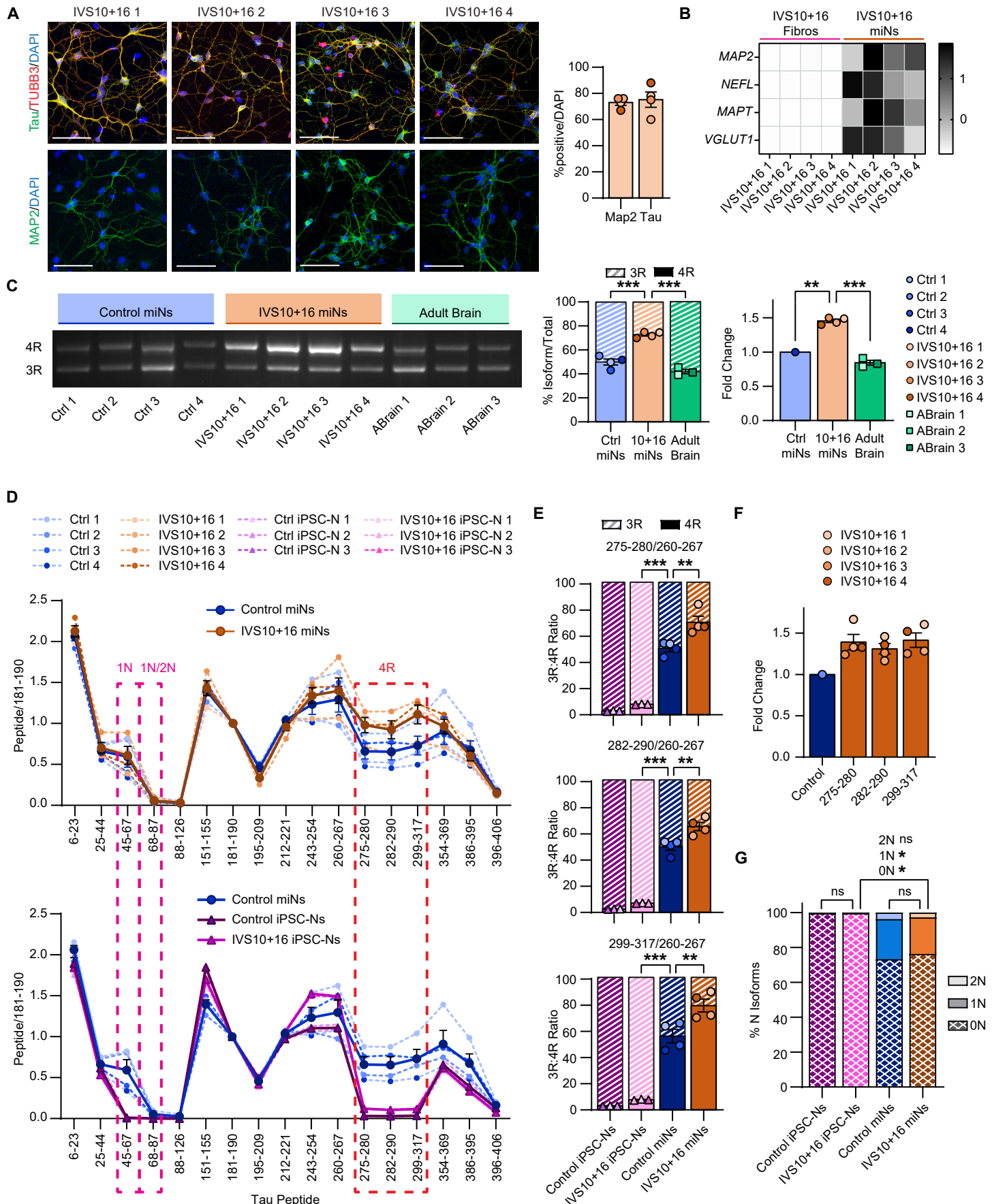
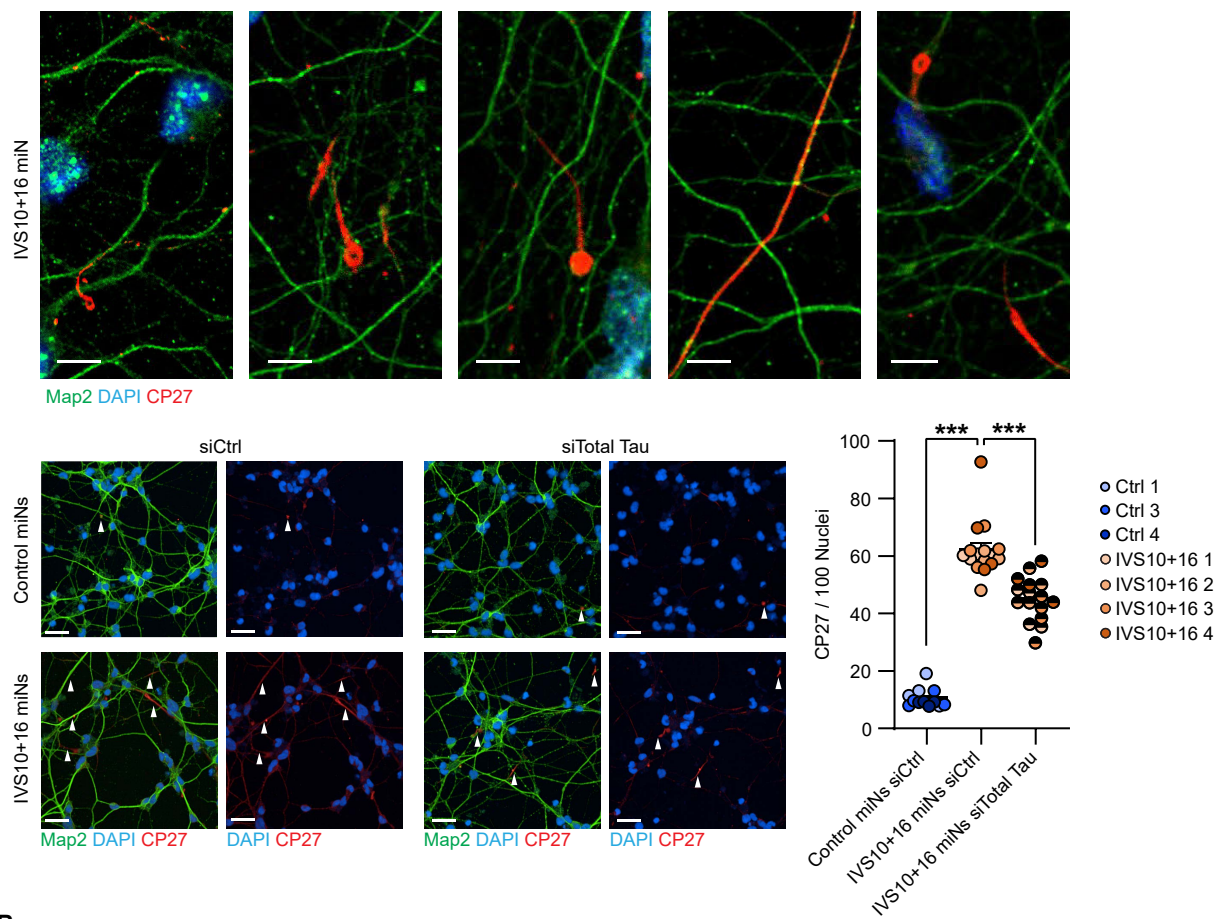
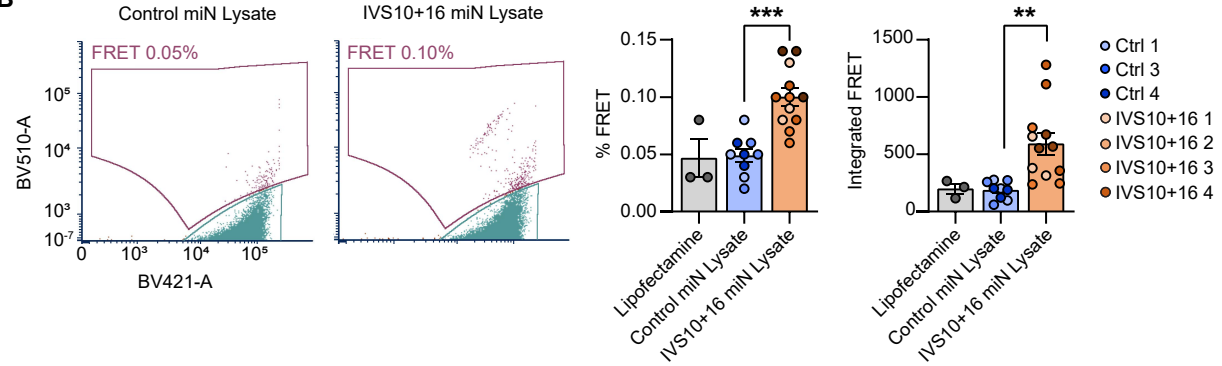


Figure 4

A

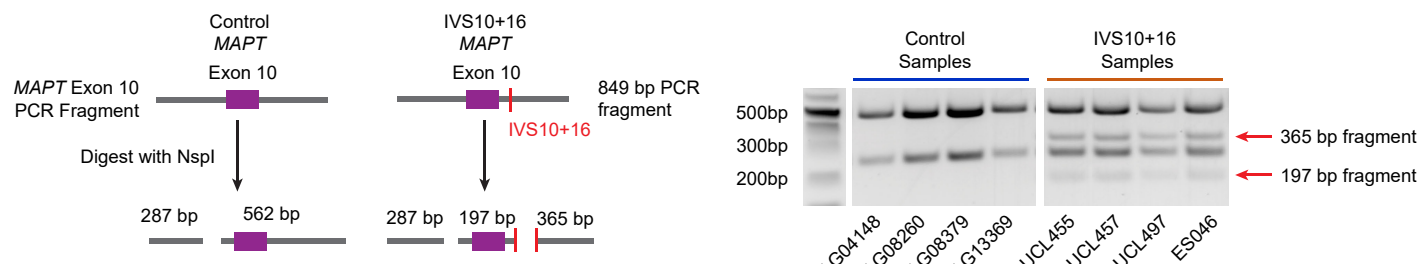


B

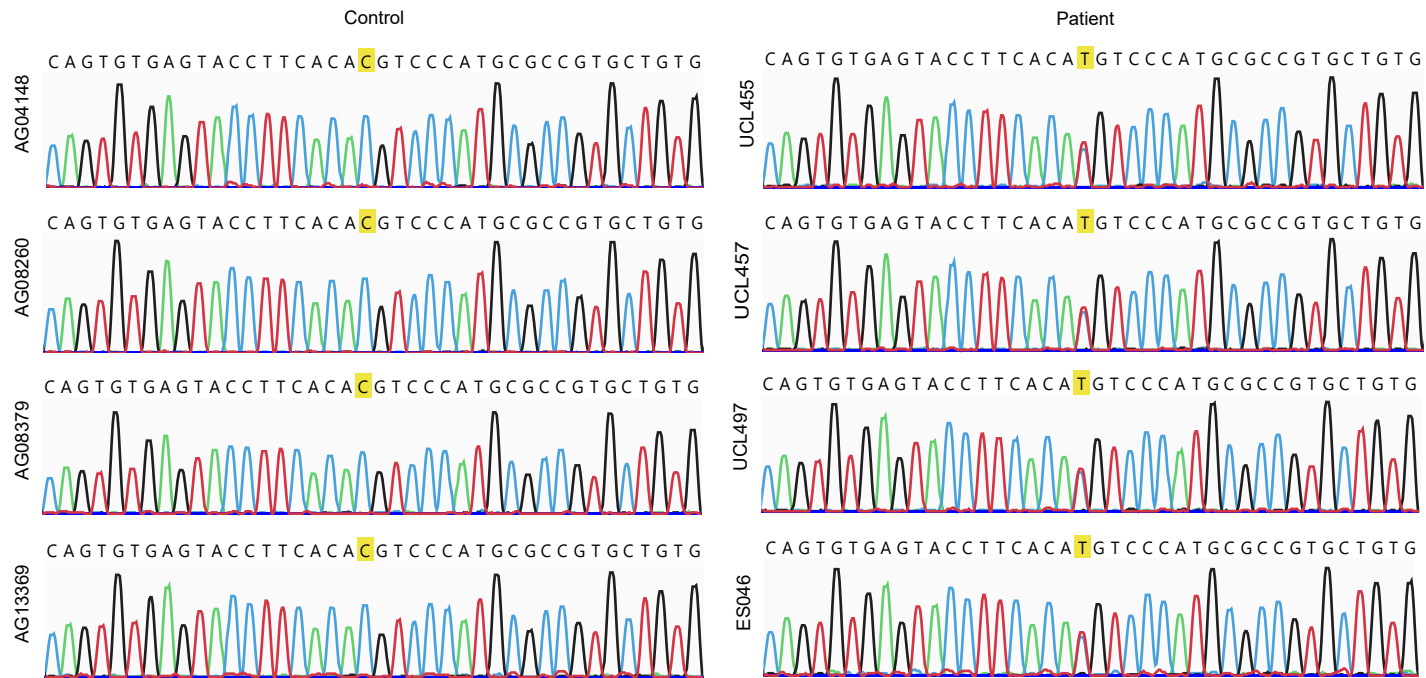


Supplemental Figure 1 | Validation of mutation status

a



b

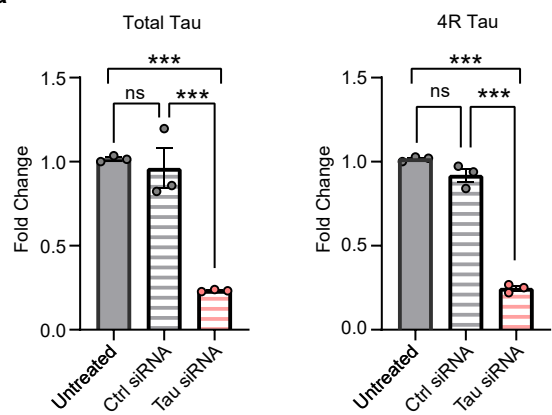


Supplemental Figure 1 | Genotyping of WT and IVS10+16 fibroblasts

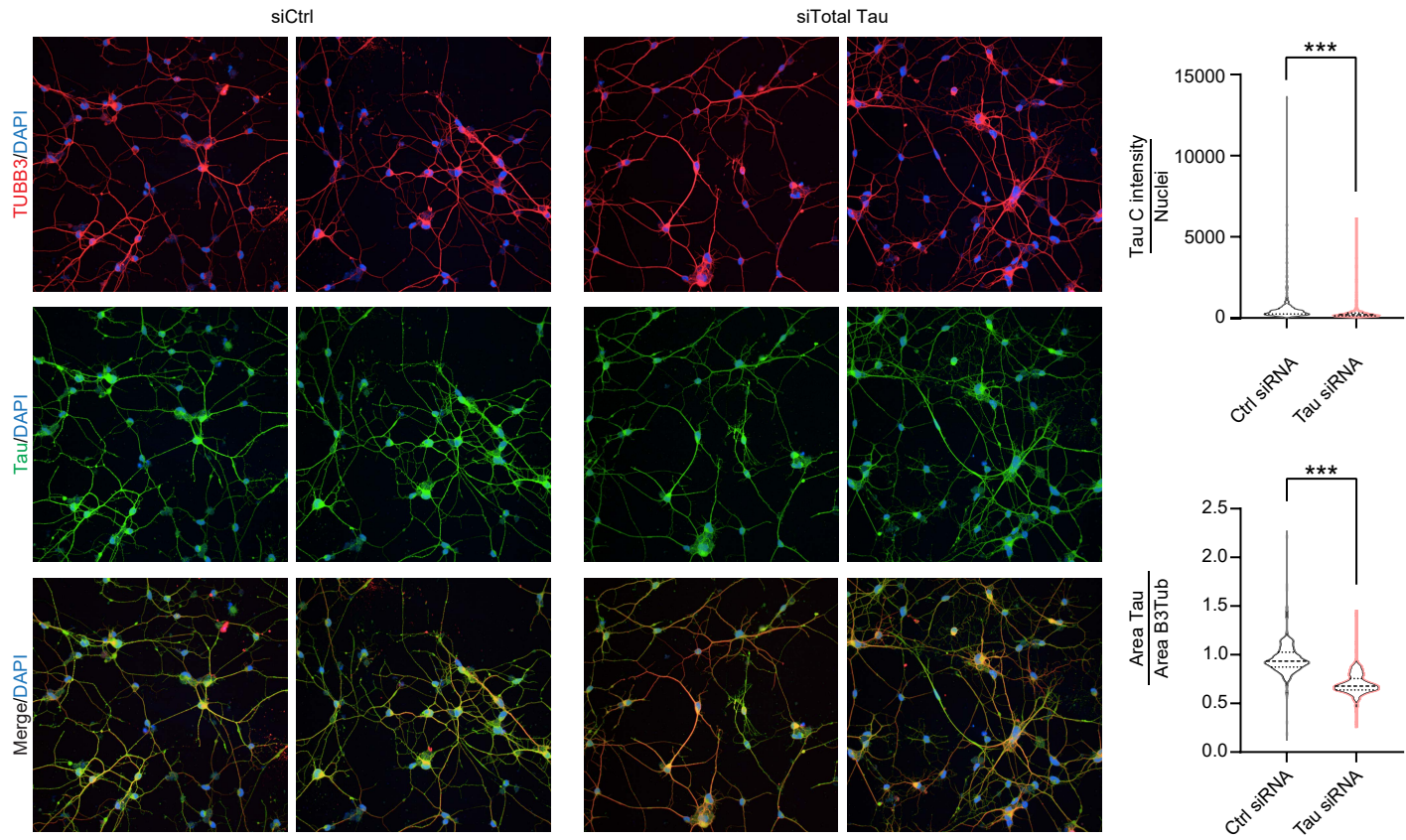
(A) Diagram explaining restriction digest genotyping for IVS10+16 C>T mutation, which creates a novel NspI site, as previously published (Hutton et al., 1998). PCR fragment is generated from genomic DNA and digested with NspI. Control samples produced 2 bands, whereas patient samples had 4. Patients are heterozygous therefore the original two bands remain. **(B)**, Sanger sequencing of MAPT in all fibroblast lines confirms the presence of IVS10+16C>T mutation in patient lines. Two peaks are present at the 10+16 location, C and T. No other MAPT mutations were present within exon 10 or in the known intronic mutation sites.

Supplemental Figure 2

a



b



Supplemental Figure 2 | Validation of reduction of total tau by siRNA

(A) qPCR of control miNs either untreated (solid grey), treated with siControl (grey stripe), or siTotal tau (pink) striped for their total tau and 4R tau expression relative to untreated. ***p < 0.001. **(B)** Immunocytochemistry of PFA-fixed control miNs treated with siControl (grey) or siTotal tau (pink) show a reduction in total tau fluorescent intensity compared to both total nuclei count and total TUBB3 area. N=389-395 images per condition. Nuclei count: siControl=9982; siTotal tau=12362. ***p < 0.001.